Accepted for publication in *the Astrophysical Journal*
Preprint typeset using LaTeX style emulateapj v. 08/22/09

arXiv:1001.0145v3 [astro-ph.SR] 17 Nov 2010

PRODUCTION OF THE p-PROCESS NUCLEI IN THE CARBON-DEFLAGRATION MODEL FOR TYPE Ia SUPERNOVAE

Motohiko Kusakabe[1], Nobuyuki Iwamoto[2], and Ken'ichi Nomoto[3]

Accepted for publication in the Astrophysical Journal

ABSTRACT

We calculate nucleosynthesis of proton-rich isotopes in the carbon-deflagration model for Type Ia supernovae (SNe Ia). The seed abundances are obtained by calculating the s-process nucleosynthesis that is expected to occur in the repeating helium shell flashes on the carbon-oxygen (CO) white dwarf (WD) during mass accretion from a binary companion. When the deflagration wave passes through the outer layer of the CO WD, p-nuclei are produced by photodisintegration reactions on s-nuclei in a region with the peak temperature ranging from 1.9 to 3.6 $\times 10^9$ K. We confirm the sensitivity of the p-process on the initial distribution of s-nuclei. We show that the initial C/O ratio in the WD does not much affect the yield of p-nuclei. On the other hand, the abundance of ^{22}Ne left after the s-processing has a large influence on the p-process via ^{22}Ne(α,n) reaction. We find that about 50% of p-nuclides are co-produced when normalized to their solar abundances in all adopted cases of seed distribution. Mo and Ru, which are largely underproduced in Type II supernovae (SNe II), are produced more than in SNe II although they are underproduced with respect to the yield levels of other p-nuclides. The ratios between p-nuclei and iron in the ejecta are larger than the solar ratios by a factor of 1.2. We also compare the yields of oxygen, iron, and p-nuclides in SNe Ia and SNe II, and suggest that SNe Ia could make a larger contribution than SNe II to the solar system content of p-nuclei.

Subject headings: Galaxy: abundances – nuclear reactions, nucleosynthesis, abundances – supernovae: general

1. INTRODUCTION

Stable nuclides of atomic number $Z \geq 34$ located at the neutron deficient side of the β-stability line are classified as p-nuclei (e.g. Lambert 1992; Meyer 1994; Arnould & Goriely 2003). They consist of 35 nuclides. The production process of these p-nuclei is commonly called the p-process. The process through the photodisintegration reactions on the pre-existing heavy nuclides is, especially, referred to as the γ-process (Woosley & Howard 1978; Howard et al. 1991). These nuclides are observed only in the solar system, since the abundances are very small, typically 1% or less in the isotopes of element (by number). Some primitive meteorites which were not in equilibrium with the bulk of the solar system materials are also found to contain very poor p-nuclei (Anders & Grevesse 1989).

Although nucleosynthetic processes to produce p-nuclei have been studied for many astrophysical sites, the core-collapse supernova (SN) of massive stars with an H-rich envelope, i.e., a Type II supernova (SN II), has been considered as a plausible site (e.g., Woosley & Howard 1978; Rayet et al. 1990; Prantzos et al. 1990; Rayet et al. 1995; Costa et al. 2000; Rauscher et al. 2002; Iwamoto et al. 2005; Hayakawa et al. 2004, 2006, 2008). During the SN explosion, the γ-process plays an important role in producing p-nuclei in the O- and Ne-rich layers.

Many studies of SNe II have shown that about a half of p-nuclides are reproduced in the proportion of the solar p-abundance. However, there remain two unresolved problems. First, ^{92,94}Mo, ^{96,98}Ru, ^{115}Sn, and ^{138}La are largely underproduced compared with the distribution of the solar p-abundances. Second, the contribution of p-nuclei from SNe II to their galactic evolution has been found to be smaller than that of ^{16}O, the main product of SNe II (Prantzos et al. 1990; Rayet et al. 1995). These results led them to conclude that SNe II could not be responsible for the whole content of solar p-nuclei.

The p-process nucleosynthesis in a supercritical accretion disk around a compact object (Fujimoto et al. 2003) and in a jet-like explosion (Nishimura et al. 2006) has been studied. Hoffman et al. (1996) suggested that nucleosynthesis in the neutrino-driven wind following the delayed explosion can produce light p-nuclei, i.e., ^{74}Se, ^{78}Kr, ^{84}Sr, and ^{92}Mo. Recently, neutrinos emitted from the collapsed core has been found to largely contribute to the production of ^{92,94}Mo, ^{96,98}Ru, and other light p-nuclei (Pruet et al. 2005; Fröhlich et al. 2006a,b; Pruet et al. 2006; Wanajo 2006). This contribution might resolve the underproduction of ^{92,94}Mo and ^{96,98}Ru in the O- and Ne-rich layers in SNe II.

Costa et al. (2000) have shown that the second problem of underproduction of p-nuclei could be solved if the $^{22}\mathrm{Ne}(\alpha,n)^{25}\mathrm{Mg}$ reaction rate was larger by a factor of $\sim$ 10–50 in the temperature range of the s-process during core He burning. However, the uncertainty they expected is too large and now questioned (Jaeger et al. 2001; Koehler 2002; Karakas et al. 2006). On the other hand, the second problem might be reconciled by considering the contribution of more energetic SNe (hypernovae) to the production of p-nuclei (Iwamoto et al.

---

[1] Institute for Cosmic Ray Research, University of Tokyo, Kashiwa, Chiba 277-8582, Japan
kusakabe@icrr.u-tokyo.ac.jp

[2] Nuclear Data Center, Japan Atomic Energy Agency, Tokai, Ibaraki 319-1195, Japan
iwamoto.nobuyuki@jaea.go.jp

[3] Institute for the Physics and Mathematics of the Universe, University of Tokyo, Kashiwa, Chiba 277-8568, Japan
nomoto@astron.s.u-tokyo.ac.jp

2005; Hayakawa et al. 2008).

It is less likely that uncertainties of the nuclear reaction rates such as (γ,n), (γ,α), and (γ,p) photodisintegrations (and their inverse reactions) for nuclei heavier than iron give a significant impact on a p-process yield as seen from the sensitivity of the p-nuclei yields on reaction rates (Rapp et al. 2006). Dillmann et al. (2008) have performed p-process calculations for the same SN II model as in Rayet et al. (1995) by utilizing most recent stellar (n,γ) cross sections. They found that overproduction factors for almost all p-nuclides decreased by, on average, 7% and that the largest deviation is the reduction in ^{156}Dy by 39.2% in comparison with the result in Rapp et al. (2006).

The p-process has also been suggested to occur in the outermost layer of the exploding carbon-oxygen (CO) white dwarf (WD) which is presumed to be a Type Ia supernova (SN Ia; Howard et al. 1991; Howard & Meyer 1992; Goriely et al. 2002; Kusakabe et al. 2005; Goriely et al. 2005; Arnould & Goriely 2006). Howard et al. (1991) calculated the p-process in a simple parametric model. In this model, it is assumed that the s-process produces seed nuclei with the mass number higher than 90 prior to the explosion. The high density environment during the passage of the shock wave makes proton capture reactions efficient in producing light p-nuclides, while the γ-process makes heavier p-nuclides. They reproduced the solar-like distribution of p-nuclei. Howard & Meyer (1992) calculated the p-process nucleosynthesis in the delayed-detonation (DD) model and obtained an abundance pattern where the abundances of lighter p-nuclei are relatively large. When the solar abundance is used for the initial composition, the result implies that SN Ia has very small contribution to the galactic content of p-nuclei. However, when the s-process is assumed to occur as in the solar metallicity asymptotic giant branch (AGB) star, a sufficient yield of p-nuclei is obtained. In this case, the underproductions of Mo and Ru are reduced, compared to those in SNe II. Those authors concluded that contribution of SN Ia on Galactic p-nuclei was still uncertain. It is, therefore, worth further studies.

Goriely et al. (2002) studied the p-process nucleosynthesis in the one-dimensional He-detonation model for a sub-Chandrasekhar mass CO WD, where the p-process would proceed in the accreting He layer. For the initial seed with solar abundances in accreting He-rich materials, the overproduction of Ca-to-Fe nuclei has been found to be a factor of ~ 100 with respect to p-nuclei. This result means that the He detonating sub-Chandrasekhar mass CO WD model is not an efficient site for the synthesis of p-nuclei. Meanwhile, they have shown that by increasing the abundances of the initial heavy seeds with the solar composition by a factor of 100 the p-nuclei yields are comparable to those of Ca-to-Fe nuclides. The resulting yields of p-nuclei in their one-dimensional model have been confirmed to be very similar to those calculated by using a three-dimensional explosion model (Goriely et al. 2005).

In light of the theoretical underproduction of ^{92,94}Mo and ^{96,98}Ru, a precise measurement of terrestrial abundances of those isotopes is needed. Recently, de Laeter (2008) has shown that the abundances of p-nuclei of Mo and Ru were, on average, 4.3% lower than presently known ones. Unfortunately, the large underproduction problem of the Mo and Ru isotopes still remains.

In this paper, we have adopted a carbon-deflagration model (W7) for SN Ia (Nomoto et al. 1984) and analyzed the p-process nucleosynthesis. The used trajectories of temperature and density in exploding WD are largely different from those in the DD model by Howard & Meyer (1992) and in the parametric model by Howard et al. (1991). It is, thus, important to investigate the C-deflagration model as one of the possible sites for the p-process. The structure of this paper is as follows. The adopted SN model, nuclear reaction network, and initial compositions are described in Section 2. The results for some cases of initial compositions are analyzed in Section 3. Finally, we present conclusions in Section 4.

2. INPUT PHYSICS

2.1. *The Supernova Model*

The adopted SN model is W7 in Nomoto et al. (1984). The accreting WD with the initial mass of 1.0 $M_\odot$ has been cooled down for 5.8×10^8 yr before the onset of mass accretion. This WD has the composition of $X(^{12}\mathrm{C}) = 0.475$, $X(^{16}\mathrm{O}) = 0.5$, and $X(^{22}\mathrm{Ne}) = 0.025$. The WD mass increases at the accretion rate of $\dot{M} = 4 \times 10^{-8}\ M_\odot\ \mathrm{yr}^{-1}$. When the WD mass approaches $M_{\mathrm{WD}} = 1.378\ M_\odot$, carbon burning is ignited at the center. This forms a C-deflagration wave which propagates outward. The released nuclear energy of about 10^{51} erg exceeds the binding energy of the WD so that the whole star is exploded. We use the time variations (trajectories) of temperature and density in the exploding layers (Nomoto et al. 1984) in order to calculate the production of p-nuclei.

We calculate the p-process nucleosynthesis in the heated layers where a peak temperature T_{m} has the range of $T_{\mathrm{m},9} = 1.86$–3.60 (in units of 10^9 K). The corresponding peak densities are $\rho_{\mathrm{m}} = 1.28 \times 10^7$ to 2.24×10^7 g cm^{-3}. These layers are located at mass coordinates of $1.143 < M_r/M_\odot < 1.280$ and undergo explosive carbon and neon burning at a passage of the deflagration wave. The representative temperature and density trajectories are shown in Figures 1(a) and 1(b), respectively. It should be noted that the yields of p-nuclei are very sensitive to the temperature and density trajectories of exploding WD. The DD and C-deflagration (W7) models show completely different characteristics of trajectories. In the W7 model, the decreasing timescale of temperature in regions of $T \gtrsim 2 \times 10^9$ K relevant to the p-process is 0.15–0.3 s, depending on mass shells. This timescale is $\sim$ 1.5–2 times longer than in the DD model by Howard & Meyer (1992) and 2–4 times shorter than in the parametric model with the assumption of e-folding time (0.6 s) by Howard et al. (1991). During the p-process nucleosynthesis, the density in W7 model is higher than in the DD model and in the assumption in Howard et al. (1991). The difference in density is also important and affects the yields of light p-nuclei resulting from proton capture reactions.

2.2. *Nuclear Reaction Network and Initial Composition*

The p-process nucleosynthesis is calculated by using the nuclear reaction network, in which 2565 nuclei from neutron and proton to Polonium ($Z = 84$) are combined with neutron, proton, α-induced reactions, and their inverses. We use the nuclear reaction rates based on the experiments and the Hauser-Feshbach statistical model, NON-SMOKER (Rauscher & Thielemann 2000). The theoretical and experimental β-decay rates are adopted from the REACLIB database (F.-K. Thielemann 1995, private communication), which are supplemented by the theoretical rates of Möller et al. (1997). We take the solar abundances from Anders & Grevesse (1989) to calculate the overproduction factor, $X/X_{\odot}$, of the produced p-nuclei, where X is the mass fraction.

The seed abundances are important to consider the nucleosynthesis by the p-process in SNe Ia. In the W7 model, materials with solar compositions are accreted onto the surface of the CO WD. The accreted H-rich materials are transformed into He through the CNO cycle of H-burning. The main product of the CNO cycle, ^{14}N, is left in the He-rich region and is processed to ^{22}Ne through the α capture reactions. The main nuclei in the CO WD result in ^{12}C, ^{16}O, and ^{22}Ne.

The accretion rate for the W7 model is high enough to avoid the occurrence of an He detonation in the sub-Chandrasekhar mass stage (Nomoto 1982a,b). Instead, He burning is ignited in a very thin shell at the base of the He-rich layer where electrons are partially degenerate. The He shell burning becomes thermally unstable in these conditions, which are similar to those in the He-burning shell of an AGB star. This results in the repeated occurrence of thermal runaway of He burning (He shell flash).

For enhanced p-process to occur in W7 model, s-process must occur when the WD mass is 1.143–1.280 $M_{\odot}$. For such high WD mass (as well as the high-mass C+O core of AGB stars), the temperature of the He-burning layer is high enough for the ^{22}Ne$(\alpha, n)^{25}$Mg reaction to take place (e.g. Fujimoto 1977; Truran & Iben 1977; Straniero et al. 2000). There is an important difference between the accreting WD and the AGB star, i.e., the mass of the H-rich layer in the accreting WD is much smaller than the AGB star and thus the entropy of the H-layer is much smaller in the WD. Therefore, the mixing of H-rich material into the He layer is more easily to occur (Sugimoto & Fujimoto 1978). Therefore, it is naturally expected that the s-process nucleosynthesis proceeds through the neutron source reactions of ^{22}Ne$(\alpha, n)^{25}$Mg as well as of ^{13}C$(\alpha, n)^{16}$O and finally creates a large amount of heavy nuclei.

The efficiency of the s-process in the accreting CO WD remains uncertain, and thus, we calculate the initial seed abundances for the p-process by using the canonical s-process model (Howard et al. 1986; Aoki et al. 2003; Terada et al. 2006). The nuclear reaction network for the s-process includes 602 nuclei connected with the neutron capture reactions, whose rates are taken from Bao et al. (2000) and Rauscher & Thielemann (2000), and the β-decays, whose rates are adopted from Takahashi & Yokoi (1987) and REACLIB. Nuclei above ^{32}S are included in the seed composition since the s-process nucleosynthesis is dominant. In this investigation, we assume two sets of initial seed abundances with mean neutron exposure $\tau_0 = 0.15$ (Case A) and 0.33 mb^{-1} (Case B) for the p-process. Figure 2 shows the seed abundance distributions normalized to the solar abundances, and Tables 1 and 2 show the seed abundances (by mass) in A and B, respectively. The seed abundance of B is fitted to the solar s-only nuclei, and thus, the distribution is similar to the solar s-distribution. The abundances of B are higher than those of A because the larger production efficiency is needed to get the constant s-distribution normalized to solar.

The He-exhausted core is composed of mainly ^{12}C and ^{16}O. The C/O abundance ratio (by mass) is assumed to be 0.95 (Case A1 in Table 3) in the W7 model. However, the C/O ratio should be changed by, e.g., the adopted reaction rate of ^{12}C$(\alpha, \gamma)^{16}$O which has a large uncertainty in the current experiments at a low energy (e.g., Makii et al. 2007). We investigate the influence of the different C/O ratio on the p-process nucleosynthesis by changing the C/O ratio from 0.56 (Case A2) to 2.55 (Case A3). The ^{22}Ne abundance left after the s-processing is also uncertain. The high abundance of ^{22}Ne may affect the p-process flows by the production of neutrons through ^{22}Ne$(\alpha, n)^{25}$Mg reaction. In order to investigate the influence, we calculate the case in which no ^{22}Ne abundance is left after the He shell flashes as an extreme case (Case A4). The ^{12}C, ^{16}O, and ^{22}Ne abundances for the adopted cases are summarized in Table 3.

3. RESULTS

3.1. *Case A1*

Here, we show the result of Case A1, which is considered as the standard case in this investigation.

3.1.1. *Abundance Variations of Light Particles, p, n, α*

Figure 3 represents the abundance variations of proton, neutron, ^{4}He, ^{12}C, ^{16}O, and ^{22}Ne in each trajectory as a function of time after the onset of explosion. In layer 1 where the peak temperature attains to $T_{\mathrm{m},9} = 3.6$, ^{16}O+^{16}O fusion reaction starts to destroy ^{16}O as the temperature increases rapidly. Layers 2–4 are the most interesting region as the main site of p-process, where explosive C and Ne burning successively occurs. ^{20}Ne first produced is photodisintegrated, and thus, ^{16}O is left (Figure 3(e)). The explosive C-burning partially operates in layer 5, but the layer is not important for the p-process. ^{22}Ne is burnt by (α, γ) and (α, n) reactions in the layers 1–4. The peak abundances of α-particle are $X_\alpha \sim 10^{-5}$ in all layers, which are larger than those in the p-process in SNe II (e.g., Prantzos et al. 1990). In the SN II model of Prantzos et al. (1990), $X_\alpha \sim 10^{-5}$ is realized by the efficient photodisintegration of ^{20}Ne at $T_9 \sim 3$, but it decreases to $X_\alpha \sim 10^{-7}$ as the peak temperatures decrease. In the SNe Ia, α particle is also produced by the ^{12}C(^{12}C, α)^{20}Ne(γ, α) in spite of no initial ^{20}Ne abundance. The peak proton and neutron abundances are $X_p \sim 10^{-7}$ and $X_n \sim 10^{-10}$, respectively, which are also larger than those in SNe II.

In the present model, neutron is produced mainly by the ^{22}Ne(α, n) reaction. The peak neutron number density is $N_n \sim 10^{22}$–10^{23} cm^{-3}, which is almost equivalent to that in the He-detonation of sub-Chandrasekhar-mass model (Goriely et al. 2002). On the other hand, the peak proton mass fraction is about five orders of magnitude smaller than that in the He-detonation model ($X_p \sim 6 \times 10^{-3}$ in the He-rich layer with $T_{\rm m,9} \gtrsim 3$). In the He-detonation model, the plenty of α-particles are present in the region where the p-process occurs and lead to the production of α-elements such as ^{40}Ca and ^{44}Ti. Further radiative α-captures bring the nuclear flow to the proton-rich side of the β-stability line, and then are followed by (α,p) reactions. This results in the very high proton mass fraction. In the C-deflagration model, on the contrary, the overproduction of proton does not take place, since the p-process occurs in outer CO-rich layers as explained below.

3.1.2. *Nuclear Flow*

The general production trends of various p-nuclei are understood through the analysis of nuclear flows. First, we see a nuclear flow in the layers with a high peak temperature. After a passage of the deflagration wave the high neutron density produced brings almost all the seed nuclei to the neutron-rich side through (n,γ) reactions. In this C-deflagration model, the abundances move to more neutron-rich region than in SNe II.[4]

(1) When the temperature exceeds $T_9 \sim 2$, (γ,n) reactions bring back the nuclear flow to the β-stability line and further to the neutron-deficient region. There is a little flow which results in a leakage to lower Z through (γ,p) and (γ,α) photodisintegrations.

(2) Furthermore, when the temperature exceeds $T_9 \sim 3$, (γ,p) and (γ,α) reactions become dominant, which drives nuclear materials from the neutron-deficient, high A region down toward the iron-peak element region. This flow to the iron-peak elements is terminated, since the photodisintegrations freeze out as the temperature of the heated layers decreases.

(3) In the layer with $T_{\rm m,9} \simeq 2.6$, the (γ,n) reactions are predominant to the seed nuclei with neutron number $N > 82$ and create the production peak for most of the p-nuclei with $N > 82$. This result is seen for ^{196}Hg in Figure 4. ^{180}Ta, which is one of the rare nuclei in nature, is produced directly through the photodisintegration of ^{181}Ta in Figure 4. We note that the production of ^{180}Ta might become efficient even in layers with lower peak temperatures ($T_{\rm m,9} = 1.8$–2.6; Prantzos et al. 1990). Unfortunately, we cannot investigate the p-process nucleosynthesis in such layers.[5]

(4) In a somewhat higher peak temperature region ($T_{\rm m,9} \sim 2.7$–2.9), (γ,n) reactions drive the nuclear flow to a sufficiently neutron-deficient region, and then, (γ,p) and (γ,α) reactions get effective to destroy seed nuclei with $N > 82$. Large amounts of heavy p-nuclei with $N > 82$ are produced in this peak temperature range from β^+-decays of unstable isobars after freezing-out of the nuclear reactions. For example, the second production peak is found for ^{196}Hg in Figure 4. The production of intermediate-mass p-nuclei with $50 < N < 82$ (especially, ^{113}In, ^{115}Sn, ^{120}Te, ^{126}Xe, ^{132}Ba, ^{138}La, and ^{136,138}Ce) already proceeds by (γ,n) photodisintegrations in this region.

(5) In the layers where the peak temperatures reach $T_{\rm m,9} \sim 2.9$–3.2, most of the intermediate-mass seed nuclei experience photodisintegrations. Then, the intermediate-mass p-nuclei are abundantly produced mainly through the β^+-decays of unstable neutron-deficient isobars.

(6) In the layers with $T_{\rm m,9} = 3.2$–3.3 ^{92,94}Mo, ^{96,98}Ru and ^{102}Pd show production peaks, but the abundances rapidly decrease when the peak temperature exceeds $T_{\rm m,9} = 3.3$. Finally, all the $N > 50$ seed nuclei are photodisintegrated to the iron-peak elements. Only $N < 50$ p-nuclides (^{74}Se, ^{78}Kr, and ^{84}Sr) are produced in the layers with $T_{\rm m,9} = 3.3$–3.6. In these hottest layers, the $^{16}{\rm O}(\gamma,\alpha)^{12}{\rm C}$ reaction produces ^{12}C, and following $^{12}{\rm C}+^{12}{\rm C}$ fusion reaction produces protons and α-particles which are identified as the second peak of their abundances in Figures 3(a) and 3(c). The synthesis of ^{74}Se, ^{78}Kr, and ^{84}Sr through proton captures, therefore, becomes effective. This results in the increases in the relative yields of the three p-nuclides and the slight increase in the mean average overproduction factor. However, we find that even at those high temperatures and even for the lightest three p-nuclei, the contribution of proton capture reactions to the production does not exceed that of photodisintegration.

3.1.3. *Yields of p-nuclei*

We calculate the overproduction factor $F = X/X_\odot$ which is the ratio between the produced abundances and the corresponding solar abundances for 35 p-nuclides in the 21 trajectories. The overproduction factors for five p-nuclides are plotted as a function of $T_{\rm m}$ in Figure 4. The selected nuclides are the same as those in Figure 3 of Prantzos et al. (1990). It is seen from Figure 4 that each nucleus is produced in a narrow range of the peak temperature.

There is one clear difference between SNe Ia and SNe II. The temperature ranges for productions of p-nuclei in SNe Ia are shifted to hotter layers than in SNe II (Prantzos et al. 1990). In addition, in the W7 model the density of the p-process site ($\sim 10^7$ g cm^{-3}) before the explosion is higher than in SNe II ($\sim 10^5$ g cm^{-3}). Thus, the number of particles (baryons) is larger in SNe Ia and the particle-induced reactions are more dominant than in SNe II. It is also the reason why neutron capture reactions, which become efficient at first in this calculation, drive the nuclear flow into the neutron-rich region far from β-stability line (Section 3.1.1.). The peak temperature, at which photodisintegration gets predominant, is thus higher in SNe Ia so that the peak temperature region, in which p-nuclei are created, totally shifts to higher one than in SNe II.

The overproduction factor averaged over the considered p-process layers is calculated for a p-nucleus by the prescription

$$\langle F \rangle = \sum_{j=2}^{N} \frac{1}{2}(F_j + F_{j-1})\frac{M_j - M_{j-1}}{M_p}, \qquad (1)$$

where F_j is the overproduction factor in a trajectory

---

[4] We checked the p-process calculation in the following approximate model of SNe II. The temperature and density are given by $T(t) = T_{\rm m}\exp(-t/3\tau_{\rm ex})$ and $\rho(t) = \rho_{\rm m}\exp(-t/\tau_{\rm ex})$, respectively, where $\tau_{\rm ex}$ is the expansion timescale taken to be 0.446 s and 1 s, and $\rho_{\rm m} = 10^6$ g cm^{-3}. This setup is the same as in Rayet et al. (1990).

[5] A mesh zoning in the outer layer of the W7 model was sparse. This is because this region is not so important for main nucleosynthesis in SN Ia.

j, M_j is the Lagrangian mass coordinate of jth trajectory, and M_p is the total mass (0.137 $M_\odot$) of the p-process layer. We define the mean overproduction factor as $F_0 = \sum_i \langle F \rangle_i / 35$, where i is a species of p-nucleus and the summation is taken for $\langle F \rangle$ values of 35 p-nuclei. Figure 5 shows the $\langle F \rangle$ values normalized to F_0, in which the filled circles represent the result for Case A1. The numerical values for these quantities are listed in Table 4.

In Case A1, 19 of 35 p-nuclides are produced in amounts within a factor of three around the mean of $F_0 = 4657$. As mentioned above, the peak temperatures of the used trajectories do not involve the range of $1.9 < T_{\mathrm{m},9} < 2.6$. Hence, some degrees of increase in yields are expected in a C-deflagration model with finer mesh zoning for nuclei of which their production yields increase in the peak temperature region of $T_{\mathrm{m},9} \leq 2.6$ (i.e., ^{138}La, ^{152}Gd, ^{156,158}Dy, ^{162,164}Er, ^{168}Yb, ^{174}Hf, ^{180}Ta, ^{184}Os, and ^{196}Hg). Taking this fact into account, ^{115}Sn might be the only p-nuclide which is markedly underproduced.

We compare the result of Case A1 with previous works. The pattern of normalized average overproduction factor $\langle F \rangle / F_0$ for p-nuclides in this calculation is very similar to that in the SNe II models (Prantzos et al. 1990; Rayet et al. 1995). For instance, the lightest three nuclides (^{74}Se, ^{78}Kr, and ^{84}Sr) are produced more than the underproduced Mo and Ru isotopes. In the intermediate-mass p-nuclides, ^{113}In and ^{115}Sn are also underabundant while the other nuclei show their nearly equal overproductions. The most remarkable difference is that in the C-deflagration model, severe underproductions of the Mo and Ru p-isotopes, which are the most puzzling problem of the p-process in SNe II (Prantzos et al. 1990; Rayet et al. 1995), are reduced by a factor of $\sim$ 6–12. However, they still remain underproduced with respect to the mean production level for 35 p-nuclei.

3.2. *Effect of the Initial Composition of the WD Core on Yields of p-nuclides*

3.2.1. *Effect of C/O Ratio*

We investigate the effect of the change in the abundance ratio between ^{12}C and ^{16}O on the p-process nucleosynthesis, keeping the initial abundances of ^{22}Ne and s-nuclei (Case A) fixed. Figure 6 shows the normalized average overproduction factors calculated for Cases A2 (stars), A1 (circles), and A3 (triangles) in the increasing order of ^{12}C/^{16}O ratio. The mean value F_0 for each case is listed in the fifth column of Table 3. For the larger C/O ratio, the relative yields of ^{74}Se, ^{78}Kr, and ^{84}Sr are larger, and those of ^{115}Sn, ^{138}La, ^{180}Ta, and ^{184}Os are smaller, although all the differences are slight. There is little variation in the overproductions F_0 (Table 3). We, thus, conclude that the nucleosynthetic results of p-process are not so sensitive to the abundance ratio between ^{12}C and ^{16}O if the ratio does not affect much the explosion timescale. It should be noted, however, that a variation of the C/O ratio could have an influence on the produced amount and pattern of p-nuclei by strongly affecting the explosion timescale.

From a comparison of the nuclear flows in Cases A1–A3, we note the following results. In layer 5 of Figure 3, partial C-burning triggers the production of protons and α-particles. The abundance of α-particle is, therefore, higher when the C/O ratio is larger. Then, the ^{22}Ne+α reaction proceeds more efficiently, so that the ^{22}Ne$(\alpha,n)^{25}$Mg reaction supplies more neutrons for larger C/O ratio.

3.2.2. *Effect of ^{22}Ne Abundance*

Second, we investigate the effect of ^{22}Ne abundance on the p-process yields by comparing the result of Case A1 with A4. In Case A4, the initial abundance of ^{22}Ne is assumed to be zero in order to examine the extreme case.

We compare the abundances of light particles in A1 with A4. The neutron abundances in A4 are 10–100 times smaller than those in A1 in the whole range of p-process layer. This is because the neutron supply through ^{22}Ne$(\alpha,n)^{25}$Mg reaction decreases due to no initial abundance of ^{22}Ne. Therefore, the nuclear flow does not reach so neutron-rich region in A4 at an early phase of the deflagration wave passage, while a larger amount of neutrons in A1 drive it to a more neutron-rich region.

The ratios of the $\langle F \rangle$ of each p-nuclide in A1 and A4 are plotted in Figure 7. It is found that ^{74}Se, ^{78}Kr, ^{84}Sr, and ^{92}Mo are produced more abundantly in A4. Since the values of F_0 except for those four nuclei are almost the same ($\sim$ 4930), their efficient productions are responsible for the increase of F_0 in A4.

Next, we investigate the differences of nuclear flow between A1 and A4. In the case of A1, ^{74}Se is created by ^{75}Se(γ,n) reaction in layer 1, but the (γ,n), (γ,p), and (γ,α) reactions photodisintegrate it. Also in layers 2–4, the ^{75}Se(γ,n) reaction produces ^{74}Se, but supplemented by ^{73}As(p,γ) reaction with a small contribution. For the production of ^{78}Kr, ^{79}Kr(γ,n) reaction is important in layer 1, but ^{78}Kr is photodisintegrated by (γ,p) reaction. In layers 2 and 3, ^{78}Kr is produced by ^{79}Kr(γ,n) reaction, together with a small contribution by ^{77}Br(p,γ) reaction. However, in layer 4 ^{77}Br(p,γ) is a main production reaction of ^{78}Kr. For ^{84}Sr, ^{85}Sr(γ,n) reaction produces it in layers 1–3, but in layer 1 (γ,n) and (γ,p) reactions destruct ^{84}Sr. In layer 4, ^{83}Rb(p,γ) and ^{85}Sr(γ,n) reactions enhance the abundance of ^{84}Sr. ^{92}Mo is created by the nuclear flow from ^{93}Mo(γ,n), ^{93}Tc(γ,p), and ^{96}Ru(γ,α) reactions, but the produced ^{92}Mo is soon destructed by (γ,p) reaction. In layers 2–4, ^{93}Mo(γ,n) reaction dominates to produce ^{92}Mo.

In contrast, the proton abundances in A4 are by a factor of $\sim$ 10 larger than those in A1. This implies that the larger amount of protons involves the production of the four p-nuclei. In the case of A4, ^{73}As(p,γ) and ^{75}Se(γ,n) reactions first create ^{74}Se in layer 1. After the peak temperature exceeds $T_9 = 3$, (γ,p), (γ,α) and (γ,n) photodisintegrations overcome the production reaction of ^{75}Se(γ,n) and destruct ^{74}Se. In layers 2–4, the contribution of ^{73}As(p,γ) reaction to the production of ^{74}Se dominates that of ^{75}Se(γ,n) and ^{75}Br(γ,p) reactions. The production of ^{78}Kr comes from ^{79}Kr(γ,n) reaction, together with minor contribution of ^{77}Br(p,γ) reaction in layer 1, but the produced ^{78}Kr is destructed by (γ,p) reaction. In layers 2–4, the ^{77}Br(p,γ) is the dominant reaction to produce ^{78}Kr, compared to ^{79}Kr(γ,n) reaction. For ^{84}Sr, the production and destruction processes in layer 1 of A4 are almost the same as in A1. However, in layers 2–4 ^{83}Rb(p,γ) reaction has also some contributions to the production of ^{84}Sr, together with ^{85}Sr(γ,n) reaction. For ^{92}Mo, the production and destruction processes in layer 1 of A4 are the same as in A1. In layers 2–4, ^{91}Nb(p,γ) reaction is important to produce ^{92}Mo and there is a small contribution of ^{93}Mo(γ,n). This result is largely different from the case of A1. Thus, proton capture reactions have an important role in the production of lightest four p-nuclides. Figure 8 shows the overproduction factor of ^{74}Se as a function of peak temperature for A1 and A4. The important contribution of proton captures to the production of ^{74}Se is found in the layer with the peak temperature $T_9 \leq 3.3$. The production region of almost all p-nuclides extends to cooler layers in A4 than in A1.

Figure 7 reveals that ^{180}Ta and ^{184}Os are underproduced in A4, compared to A1. The abundance peak of these two p-nuclei in A1 is found to be in the layer with $T_{\mathrm{m},9} = 2.6$.[6] In the layer, ^{180}Ta is first created by ^{181}Ta(γ,n) reaction, which is later destructed by ^{180}Ta(γ,n) reaction as the temperature increases to its peak. The production and destruction timescales of ^{180}Ta depend on the inverse reactions. This is because the nuclear flow from ^{180}Ta to ^{179}Ta depends on the rates of ^{180}Ta(γ,n) and ^{179}Ta(n,γ) reactions. The reaction rate of photodisintegration is a function of temperature only. However, the reaction rate of neutron capture is dependent on the temperature, density, and neutron abundance which is larger in A1 than in A4. Thus, the contribution of neutron capture reactions in A1 is more important than in A4, and the destruction timescale of ^{180}Ta in A1 is longer than in A4. These facts lead to a larger abundance of ^{180}Ta in A1 left after the termination of nuclear processing.

The situation for the production of ^{184}Os is similar to that for ^{180}Ta. The production and destruction processes of ^{184}Os are the competition between photodisintegrations on ^{184}Os and ^{185}Os and neutron capture reactions on ^{183}Os and ^{184}Os. The nuclear flux of ^{185}Os$(\gamma,n)^{184}$Os$(\gamma,n)^{183}$Os in A1 is relatively small due to a larger amount of neutrons than in A4. In addition, ^{183}Os(n,γ) creates ^{184}Os in the later phase of explosion in A1. As a result, the final abundance of ^{184}Os is by a factor of 15 larger in A1.

3.3. *Effect of the Initial Abundances of s-nuclei on Yields of p-nuclei*

Here, we examine the impact of different seed distributions of Cases A (A1–A4) and B with the enhancement from the solar abundance of heavy nuclei. In this investigation, we compare A1 with B, which has similar abundances to A1 for ^{12}C, ^{16}O, and ^{22}Ne in the CO core.

Figure 2 shows that the overabundances of s-nuclei in Case B are by factors of 10–100 larger than those in A. Especially, in B heavy seed s-nuclei with $A > 140$ are about 100 times more abundant than in A. This leads to the increase of F_0 by a factor of 50 in B, relative to A. This increase is seen for each p-nuclide in Figure 5, in which the normalized $\langle F \rangle$ is presented for Cases A1 and B. The values of normalized $\langle F \rangle$ for heavy p-nuclei with $A > 140$, especially ^{168}Yb, ^{174}Hf, ^{180}W, and ^{196}Hg, are larger than those in A. In contrast, lighter p-nuclei have smaller values in B than those in A. In particular, ^{74}Se–^{98}Ru shows significant reductions, which come from the decrease in relative abundances of seed nuclei near the p-nuclei, compared to heavy seed nuclei with $A > 140$.

The resulting distribution of p-nuclei shows important decreases in ^{74}Se–^{98}Ru as seen in B, if the distribution of heavy seed s-nuclei is similar to that of the solar distribution. This result is analogous to that obtained by the p-process in SNe II, but with the even worse reduction of ^{74}Se–^{84}Sr. Thus, we find that the distribution similar to that of the solar p-nuclei is obtained by the seed distribution attributed to the s-process under an environment with metallicity close to solar (Gallino et al. 1998), although main neutron source might be ^{22}Ne(α,n) reaction.

The presupernova abundance of s-nuclei in the WD thus has a large impact on the p-process nucleosynthesis and is very crucial for the resulting yields of p-nuclei.

3.4. *Contribution of C-deflagration SNe to the Galactic Yields of p-nuclei*

The biggest question concerning the p-process nucleosynthesis is where the main production site is. In order to investigate this question, we estimate the contribution of SN Ia to galactic chemical evolution of p-nuclei by comparing the ejected mass of ^{56}Fe, a main product of SN Ia, with those of p-nuclei in Case A1.

Here, we introduce a *net yield* of each nuclide in SNe Ia, defined as a difference between the mass of the nuclide returned to the interstellar space at the SN explosion and the mass engulfed into a star at its birth. The p-nuclei present at the star formation remain inside the p-process layer before the explosion, but they are destroyed by photodisintegrations. In addition, we assume that the p-nuclei present in an accreted matter are burned by neutron capture during the s-process developing in the He intershell (see, e.g., Tables 1 and 2). Therefore, the p-nuclei ejected from the SN Ia explosion are only those ultimately produced in the p-process layer.

Assuming that the mass of CO core in the WD is approximately equal to that of the whole WD, the net yield for p-nuclide i is given by

$$y_i = X_{i,\odot}(\langle F \rangle_i M_p - M_{\mathrm{WD}}), \tag{2}$$

where $M_{\mathrm{WD}} = 1.378 M_\odot$ is the mass of the WD (Nomoto et al. 1984) and $X_{i,\odot}$ is the solar mass fraction of p-nuclide i. The above prescription could also be applied to ^{56}Fe, so that the net yield of ^{56}Fe is

$$y_{^{56}\mathrm{Fe}} = X_{^{56}\mathrm{Fe},\odot}(M_{^{56}\mathrm{Fe}}/X_{^{56}\mathrm{Fe},\odot} - M_{\mathrm{WD}}), \tag{3}$$

where $M_{^{56}\mathrm{Fe}}$ is the mass of ^{56}Fe ejected by an SN Ia and $X_{^{56}\mathrm{Fe},\odot} = 1.17 \times 10^{-3}$ is the solar mass fraction of ^{56}Fe. By taking a ratio between these quantities normalized to the corresponding solar mass fraction for respective nuclides, we can evaluate how many SN Ia events contribute to the galactic chemical evolution of one nuclide. The calculated ratio of yields between ^{56}Fe and a representative p-nucleus is as follows:

---

[6] The zoning of W7 model in the outermost layer is relatively coarse. If the finer zones were used, the abundance peak of ^{180}Ta and ^{184}Os would appear in the outer layer where $T_{\mathrm{m},9}$ would be lower than 2.6.

$$^{56}\mathrm{Fe}/p \equiv \frac{y_{^{56}\mathrm{Fe}}/X_{^{56}\mathrm{Fe},\odot}}{(1/35)\sum_{i=1}^{35} y_i/X_{i,\odot}} = \frac{M_{^{56}\mathrm{Fe}}/X_{^{56}\mathrm{Fe},\odot} - M_{\mathrm{WD}}}{F_0 M_p - M_{\mathrm{WD}}} \quad (4)$$

where the yield of the p-nucleus is derived by summing the net yields of each p-nuclide and averaging it over 35 p-nuclei.

The yield ratio ($^{16}\mathrm{O}/p$) between ^{16}O and the representative p-nucleus is also defined in the same way, in which the solar mass fraction of ^{16}O is assumed to be $X_{^{16}\mathrm{O},\odot} = 9.59 \times 10^{-3}$. In this C-deflagration model for an SN Ia, we obtain $^{56}\mathrm{Fe}/p = 0.82$ and $^{16}\mathrm{O}/p = 0.023$ for Case A1 (Tsujimoto et al. 1995). These results indicate that p-nuclei are produced more than ^{56}Fe and ^{16}O when normalized to their solar abundances. We, therefore, conclude that SNe Ia can account for the galactic content of p-nuclei assuming that the seed s-nuclei are produced efficiently up to the overproduction level of $\sim 10^3$ in He-rich layer accreting onto the degenerate CO WD.

3.5. *Comparison with Previous p-process Calculations*

Goriely et al. (2002) calculated p-process nucleosynthesis in the sub-Chandrasekhar mass He-detonation model. The stable nuclei from Ca to Fe are overabundant with respect to p-nuclei by a factor of ~ 100. They, therefore, concluded that the He-detonation model is not an efficient site for production of p-nuclei. Nevertheless, Goriely et al. claimed that if the initial abundances of s-nuclei are enhanced over their solar values by a factor of 100, p-nuclei are produced at the same level as Ca–Fe, while such enhancement of the s-nuclei is not trivial in the He-detonation model. On the other hand, in the present C-deflagration model the overproduction factors for ejected p-nuclides and stable nuclides lighter than Fe-group elements are plotted as a function of mass number in Figure 9 and are listed in Table 5. From this figure, it is found that $F_{\mathrm{Ca\text{-}Fe}} \sim F_p$ is realized with some enhancements of heavy seed nuclei, which are a natural consequence from the accretion of H-rich matter onto a CO WD with an appropriate rate of mass accretion, although the enhancement level of heavy seed nuclei remains ambiguous. This means that the C-deflagration model is $\sim$100 times more effective in enriching a galaxy with p-nuclei, if the assumed level of enhancement is valid.

As mentioned in Section 1, the DD model for SNe Ia may also produce an important amount of p-nuclei if the prior enhancement of s-nuclei in a Chandrasekhar mass WD model is taken into account (Howard & Meyer 1992) as in our present assumptions. However, the enhancement of s-nuclei is not trivial for the double degenerate scenario of SN Ia in a Chandrasekhar mass model.

Arnould & Goriely (2003) have calculated the p-process nucleosynthesis in the W7 model for SNe Ia adopting two cases as an initial abundance of heavy seed nuclei. The resulting pattern of yields of p-nuclei in Arnould & Goriely (2003) under the assumption of the solar abundance for initial seed shows the following difference from our Case A. Normalized abundances of p-nuclei for Mo–Ce in Arnould & Goriely (2003) are much smaller, but those for heavier p-nuclei are larger. This trend represents the solar abundance of p-nuclei themselves. On the other hand, their result for the initial seed distribution representative of the s-process in AGB stars of the solar metallicity is similar to that of Case A. It is, however, found that there exists a difference of the pattern between our Case A and Arnould & Goriely (2003) for p-nuclei with $N > 82$, while the pattern for p-nuclei with $N \leq 82$ is similar. This result represents that the abundance pattern for heavier p-nuclei is very sensitive to initial seed distributions. It should be noted that the differences in yields of ^{113}In, ^{158}Dy, and ^{190}Pt are larger than those within nuclear uncertainties evaluated by Arnould & Goriely (2003).

Prantzos et al. (1990) studied the p-process in SNe II using the model for SN1987A, and obtained F_{O}/F_p ($\approx ^{16}\mathrm{O}/p$) ~ 12, where F_{O} stands for the overproduction factor of oxygen. They claimed that the solar system content of p-nuclei does not come from SN1987A-like SNe. One reason may be attributed to the abundances of seed nuclei which reflect low metallicity in the Large Magellanic Cloud. Rayet et al. (1995) derived the ratios of yields for oxygen and p-nuclei from star models with masses of 13, 15, 20, and 25 $M_\odot$ and averaged them over the initial mass function (IMF). They found that the resulting ratio was $F_{\mathrm{O}}/F_p = 4.2$. These results, thus, imply that p-nuclei are not sufficiently produced, compared to the main product in SNe II and suggest that the other production sites have an important contribution to the galactic evolution of p-nuclei. Accordingly, the C-deflagration model for SNe Ia is one of the promising sites for the p-process because sufficient amounts of p-nuclei are produced relative to ^{16}O within our assumptions.

Using the results of this study and previous works, we estimate how many SNe Ia and SNe II contribute to the galactic evolution of p-nuclei. We assume that all SNe Ia would typically experience the p-process as in Case A1. First, we adopt the ratios of overproduction factors $^{56}\mathrm{Fe}/p = 0.82$ for our SN Ia model and $^{16}\mathrm{O}/p = 4.2$ for SNe II (Rayet et al. 1995). We also take the ejected masses of ^{16}O and ^{56}Fe from the W7 model for SN Ia and the IMF-averaged masses of these nuclides from SNe II (Tsujimoto et al. 1995). These masses normalized to the corresponding solar abundances are summarized in Table 6. Values for p-nuclei are estimated from the yield ratios between p-nuclei and the main products (^{56}Fe for SN Ia and ^{16}O for SN II). In order to compare these yields between SN Ia and SN II, we adopt the ratio of the occurrence frequency of SNe Ia to that of SNe II, ~ 0.15 (Tsujimoto et al. 1995). From the values in Table 7, we find that SNe Ia contribute about 70% of the p-nuclei in the solar system. It should be noted that there is still a small underproduction of p-nuclei with respect to ^{16}O, i.e., $^{16}\mathrm{O}/p = 2/1.46 = 1.4$, while the ratio of the yields between ^{56}Fe and p-nuclei almost agrees with that of the solar abundance, i.e., $^{56}\mathrm{Fe}/p = 1.57/1.46 = 1.1$.

4. CONCLUSIONS

We calculate the p-process nucleosynthesis in the carbon-deflagration model for SNe Ia (W7 model in Nomoto et al. 1984) with realistic initial abundances of s-nuclei. The temperature and density trajectories in W7 are different from those of the DD model adopted in Howard & Meyer (1992) and the parameter study (Howard et al. 1991). The adopted *s*-process patterns are also different from the previous study. We investigate the effects on productions of *p*-nuclei of (1) the different initial ^{12}C abundances which affect the explosive C-burning, (2) the uncertain initial abundance of ^{22}Ne at the explosion, whose (α, n) reaction is an important neutron source for the *s*-process occurring during the He shell flashes, and (3) the different distributions in the *s*-process which provides initial seed abundances for the *p*-process. Our findings are summarized as follows.

1. In all cases we considered, more than 50% of *p*-nuclides are co-produced at almost the same degree of enhancements with respect to their solar abundances. We find that SNe Ia can produce Mo and Ru *p*-isotopes $\sim$ 6–12 times more in Case A1 than SNe II on the basis of the mean overproduction factor of *p*-nuclei, although the problem of the relative underproduction still remains. The patterns of *p*-nuclei obtained in this study are different from those in Howard & Meyer (1992) and Howard et al. (1991), reflecting the differences in temperature and density profiles and initial distribution of seed nuclei. In addition, it is confirmed that the *p*-process layer in this C-deflagration model shifts to a higher temperature region than that in SNe II.

2. The effect of variable C/O ratio in the initial composition of the CO WD on the *p*-nuclei yields is small. On the other hand, the effect of the initial ^{22}Ne abundances is large especially for ^{74}Se, ^{78}Kr, ^{84}Sr, and ^{92}Mo. If the initial ^{22}Ne is less abundant, the light *p*-nuclides are enhanced. In order to produce enough Mo and Ru *p*-isotopes, the abundance of ^{22}Ne smaller than the assumption in W7 model is expected. Initial abundances of various nuclides other than ^{12}C, ^{16}O, and ^{22}Ne considered in this study also affect the *p*-process through supplies of neutron, proton, and α-particle emerging during the explosion.

3. The effect of initial abundances of *s*-nuclei on the *p*-process is large. If the *s*-process efficiently contributes to the production of seed nuclei, yields of *p*-nuclei increase and relative yields of heavy *p*-nuclei are enhanced more than those of lighter ones. Such enhancement of *s*-nuclei is expected for the single degenerate scenario of the Chandrasekhar mass model, but not trivial in the double degenerate scenario.

4. This result leads to a possibility that SNe Ia play an important role in the galactic evolution of *p*-nuclei. The *p*-nuclei are produced by a factor of $\sim$ 1.2 more than ^{56}Fe when normalized to the solar abundances. SNe Ia, therefore, may have contributed to the enrichment of *p*-nuclei more effectively than SNe II (about twice in Case A1). Our calculation involves an uncertainty in the initial abundances of nuclides (e.g., ^{22}Ne) in the C-deflagration model of the exploding CO WD. This has a great influence on abundances of background particles, i.e., protons, neutrons, and α-particles in the *p*-process nucleosynthesis. There is also an important uncertainty in the *s*-process in presupernova stars which affects initial distributions of the *s*-nuclei and the remaining ^{22}Ne abundance. Studies of the *s*-process nucleosynthesis during the presupernova evolution of accreting WDs are necessary to clarify if the *p*-process in SNe Ia could really produce enough abundances of *p*-nuclei. Despite these uncertainties, the present study strongly suggests that SNe Ia, as well as SNe II, could be a probable production site of the solar *p*-nuclei.

This work has been supported by Grant-in-Aid for the Japan Society for the Promotion of Science (JSPS) Fellows (21.6817), and for Scientific Research of JSPS (18104003, 18540231, 20244035, 20540226) and the Ministry of Education, Culture, Sports, Science, and Technology (MEXT; 19047004, 20040004). This work has also been supported by World Premier International Research Center Initiative, MEXT, of Japan.

REFERENCES

Anders, E., & Grevesse, N. 1989, Geochim. Cosmochim. Acta, 53, 197

Aoki, W., et al. 2003, ApJ, 592, L67

Arnould, M., & Goriely, S. 2003, Phys. Rep., 384, 1

Arnould, M., & Goriely, S. 2006, Nucl. Phys. A, 777, 157

Bao, Z. Y., Beer, H., Käppeler, F., Voss, F., Wisshak, K., & Rauscher, T. 2000, At. Data Nucl. Data Tables, 76, 70

Costa, V., Rayet, M., Zappalà, R. A., & Arnould, M. 2000, A&A, 358, L67

de Laeter, J. R. 2008, Phys. Rev. C, 77, 045803

Dillmann, I., Rauscher, T., Heil, M., Käppeler, F., Rapp, W., & Thielemann, F.-K. 2008, J. Phys. G: Nucl. Part. Phys., 35, 014029

Fröhlich, C., Martínez-Pinedo, G., Liebendörfer, M., Thielemann, F.-K., Bravo, E., Hix, W. R., Langanke, K., & Zinner, N. T. 2006a, Phys. Rev. Lett., 96, 142502

Fröhlich, C., et al. 2006b, ApJ, 637, 415

Fujimoto, M. Y. 1977, PASJ, 29, 537

Fujimoto, S., Hashimoto, M., Koike, O., Arai, K., & Matsuba, R. 2003, ApJ, 585, 418

Gallino, R., Arlandini, C., Busso, M., Lugaro, M., Travaglio, C., Straniero, O., Chieffi, A., & Limongi, M. 1998, ApJ, 497, 388

Goriely, S., García-Senz, D., Bravo, E., & José, J. 2005, A&A, 444, L1

Goriely, S., José, J., Hernanz, M., Rayet, M., & Arnould, M. 2002, A&A, 383, L27

Hayakawa, T., Iwamoto, N., Kajino, T., Shizuma, T., Umeda, H., & Nomoto, K. 2006, ApJ, 648, L47

Hayakawa, T., Iwamoto, N., Kajino, T., Shizuma, T., Umeda, H., & Nomoto, K. 2008, ApJ, 685, 1089

Hayakawa, T., Iwamoto, N., Shizuma, T., Kajino, T., Umeda, H., & Nomoto, K. 2004, Phys. Rev. Lett., 93, 161102

Hoffman, R. D., Woosley, S. E., Fuller, G. M., & Meyer, B. S. 1996, ApJ, 460, 478

Howard, W. M., Mathews, G. J., Takahashi, K., & Ward, R. A. 1986, ApJ, 309, 633

Howard, W. M., & Meyer, B. S. 1992, in Nuclei in the Cosmos Symp. 2, ed. F. Käeppeler & K. Wisshak (Bristol: Institute of Physics Publishing), 575

Howard, W. M., Meyer, B. S., & Woosley, S. E. 1991, ApJ, 373, L5

Iwamoto, N., Umeda, H., & Nomoto, K. 2005, in Origin of Matter and Evolution of Galaxies 2003, ed. M. Terasawa et al. (Hackensack, NJ: World Scientific), 493

Jaeger, M., Kunz, R., Mayer, A., Hammer, J. W., Staudt, G., Kratz, K. L., & Pfeiffer, B. 2001, Phys. Rev. Lett., 87, 202501

Karakas, A. I., Lugaro, M. A., Wiescher, M., Görres, J., & Ugalde, C. 2006, ApJ, 643, 471

Koehler, P. E. 2002, Phys. Rev. C, 66, 055805

Kusakabe, M., Iwamoto, N., & Nomoto, K. 2005, Nucl. Phys. A, 758, 459

Lambert, D. L. 1992, A&AR, 3, 201

Makii, H., Nagai, Y., Mishima, K., Segawa, M., Shima, T., & Igashira, M. 2007, Phys. Rev. C, 76, 022801

Meyer, B. S. 1994, ARA&A, 32, 153

Möller, P., Nix, J. R., & Kratz, K.-L. 1997, At. Data Nucl. Data Tables, 66, 131

Nishimura, N., Hahimoto, M., Fujimoto, S., Kotake, K., & Yamada, S. 2006, AIP Conf. Proc. 847, in Origin of Matter and Evolution of Galaxies, ed. S. Kubono et al. (Melville, NY: AIP), 452

Nomoto, K. 1982a, ApJ, 253, 798

Nomoto, K. 1982b, ApJ, 257, 780

Nomoto, K., Thielemann, F. K., & Yokoi, K. 1984, ApJ, 286, 644

Prantzos, N., Hashimoto, M., Rayet, M., & Arnould, M. 1990, A&A, 238, 455

Pruet, J., Hoffman, R. D., Woosley, S. E., Janka, H.-T., & Buras, R. 2006, ApJ, 644, 1028

Pruet, J., Woosley, S. E., Buras, R., Janka, H.-T., & Hoffman, R. D. 2005, ApJ, 623, 325

Rapp, W., Görres, J., Wiescher, M., Schatz, H., & Käppeler, F. 2006, ApJ, 653, 474

Rauscher, T., Heger, A., Hoffman, R. D., & Woosley, S. E. 2002, ApJ, 576, 323

Rauscher, T., & Thielemann, F.-K. 2000, At. Data Nucl. Data Tables, 75, 1

Rayet, M., Arnould, M., Hashimoto, M., Prantzos, N.,& Nomoto., K. 1995, A&A, 298, 517

Rayet, M., Prantzos, N., & Arnould, M. 1990, A&A, 227, 271

Straniero, O., Limongi, M., Chieffi, A., Dominguez, I., Busso, M., & Gallino, R. 2000, Mem. Soc. Astron. Ital., 71, 719

Sugimoto, D., & Fujimoto, M. Y. 1978, PASJ, 30, 467

Takahashi, K., & Yokoi, K. 1987, At. Data Nucl. Data Tables, 36, 375

Terada, K., Itoh, K., Hidaka, H., Yoshida, T., Iwamoto, N., Aoki, W., & Williams, I. S. 2006, New Astron. Rev., 50, 582

Truran, J. W., & Iben, I., Jr. 1977, ApJ, 216, 797

Tsujimoto, T., Nomoto, K., Yoshii, Y., Hashimoto, M., & Yanagida, S. 1995, MNRAS, 277, 945

Wanajo, S. 2006, ApJ, 647, 1323

Woosley, S. E., & Howard, W. M. 1978, ApJS, 36, 285

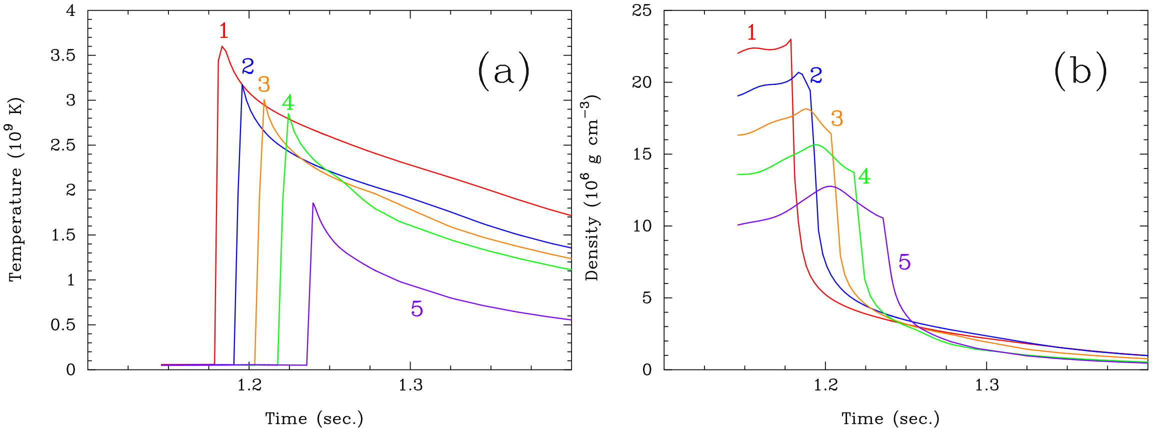

Figure 1. Trajectories of temperature (a) and density (b) as a function of time in the W7 model. The labels refer to the trajectories in the layers with the peak temperatures in units of 10^9 K, i.e., $T_{\mathrm{m},9} = T_\mathrm{m}/(10^9\ \mathrm{K}) = 3.60$ (1), 3.17 (2), 3.01 (3), 2.85 (4), and 1.86 (5).

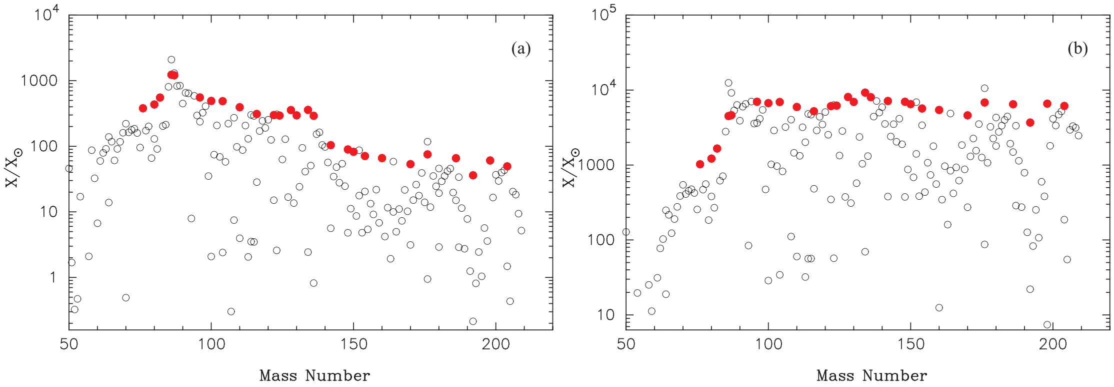

Figure 2. Distributions of initial seed abundances relative to solar for Case A (a) and B (b) (Table 3), respectively. Filled circles indicate *s*-only nuclides.

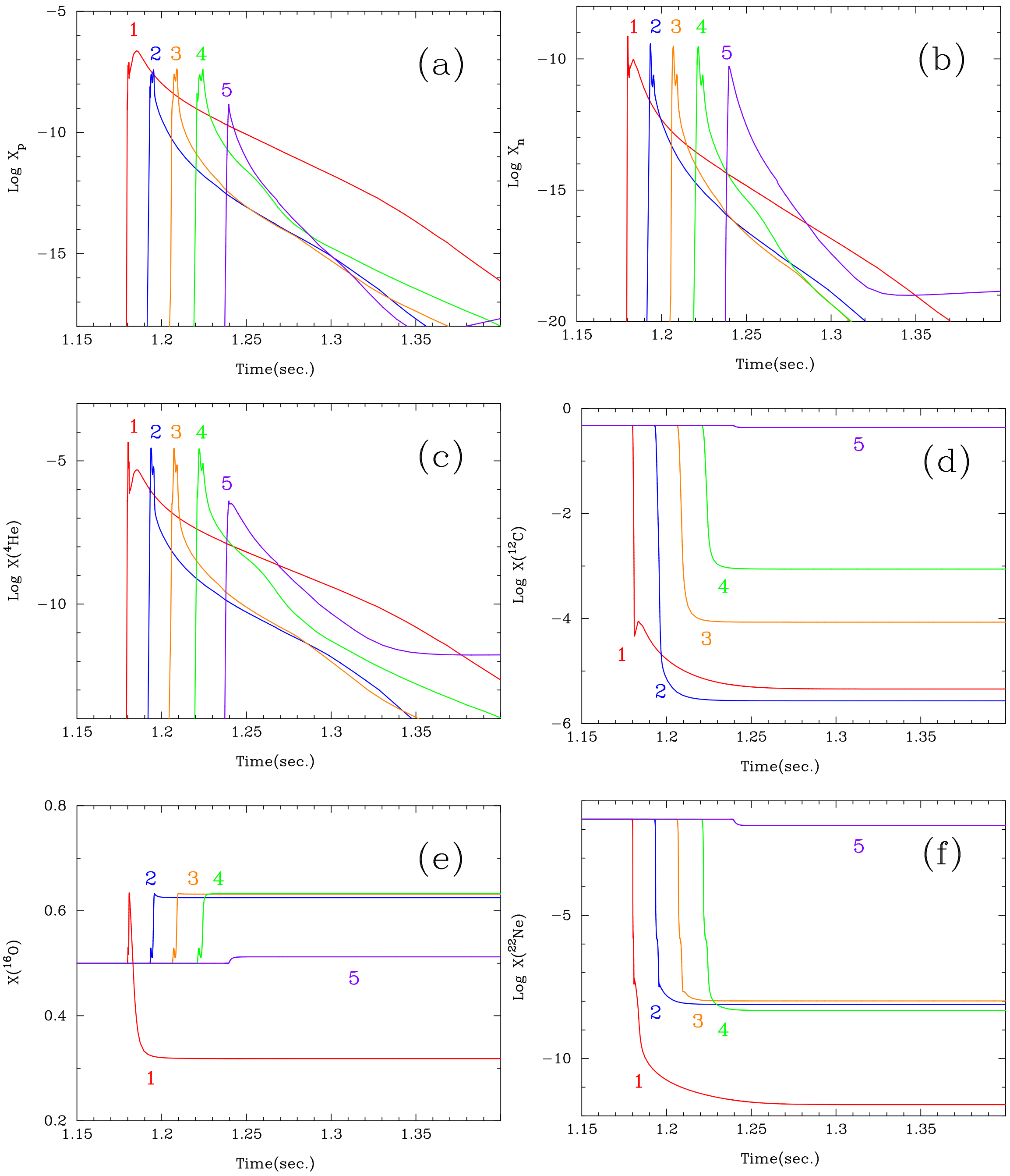

Figure 3. Time evolution of mass fractions of proton (a), neutron (b), ^{4}He (c), ^{12}C (d), ^{16}O (e), and ^{22}Ne (f) during the explosion in the five layers shown in Figure 1.

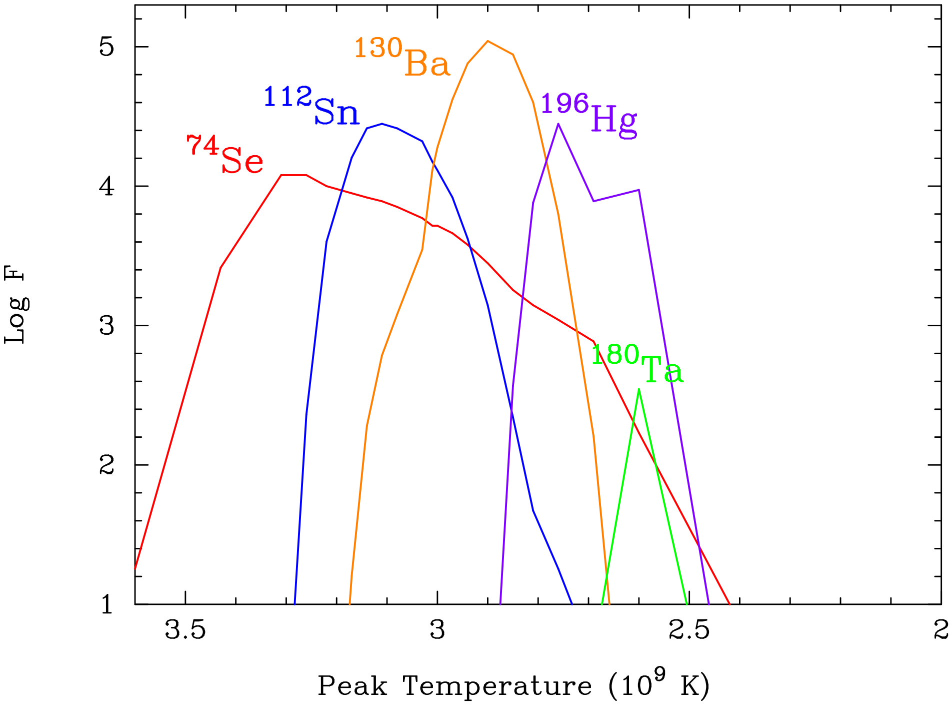

Figure 4. Dependence of the production of representative *p*-nuclei (^{74}Se, ^{112}Sn, ^{130}Ba, ^{180}Ta, and ^{196}Hg) on the peak temperature $T_{\rm m}$.

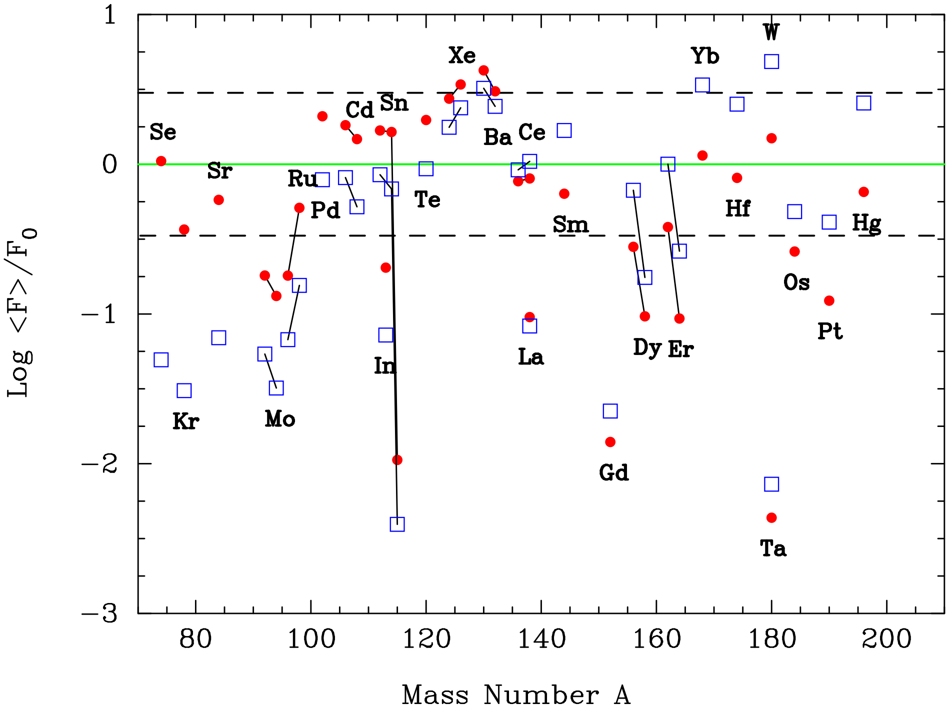

Figure 5. Average overproduction factors $\langle F\rangle$ normalized to F_0 for the *p*-nuclides as a function of mass number. The results of Cases A1 and B (Table 3) are shown by filled circles and open squares, respectively. Horizontal solid and dashed lines correspond to $\langle F\rangle/F_0 = 1$ and (3, 1/3), respectively.

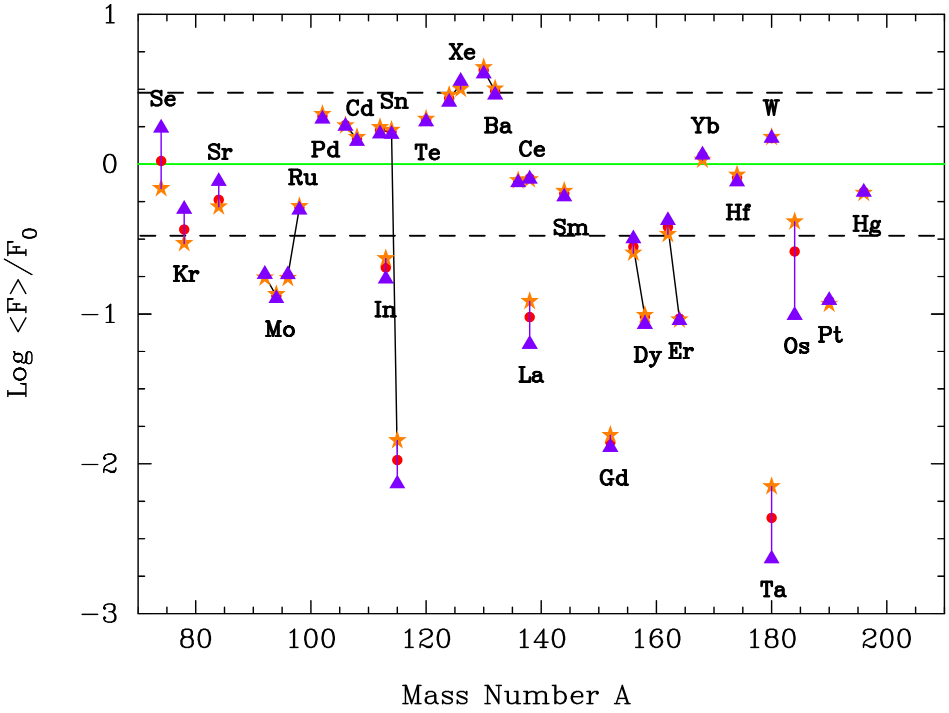

Figure 6. Average overproduction factors normalized to F_0 for three initial compositions: Cases A1 (circles), A2 (stars), A3 (triangles; Table 3).

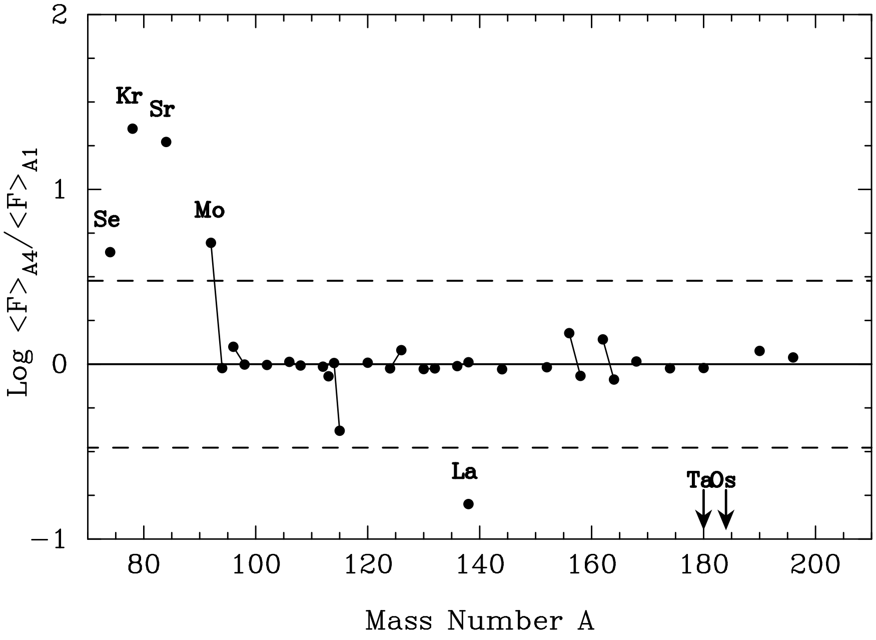

Figure 7. Average overproduction factors in Case A4 with respect to those in Case A1 (Table 3), i.e., $\langle F\rangle_{\rm A4}/\langle F\rangle_{\rm A1}$ for p-nucleus.

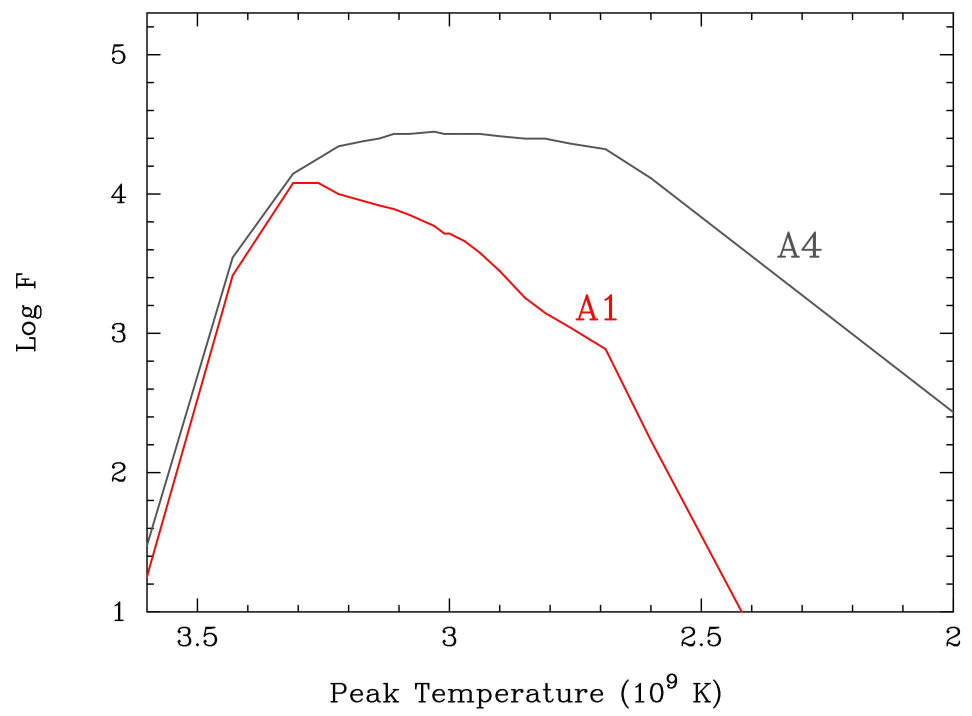

Figure 8. Overproduction factors of ^{74}Se as a function of peak temperature for Cases A1 and A4.

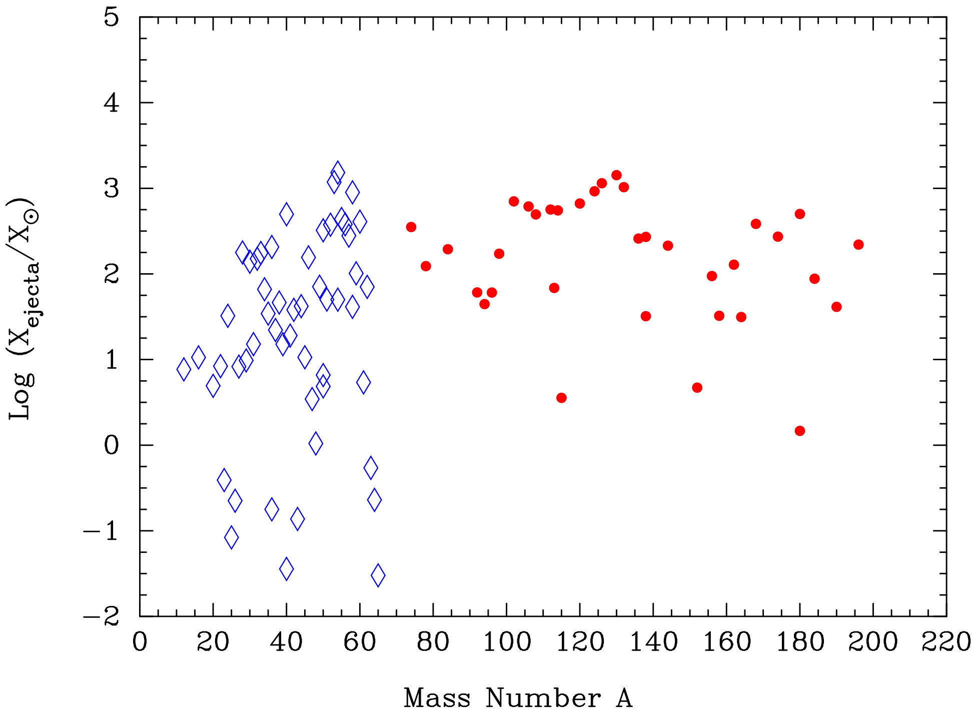

Figure 9. Overproduction of *p*-nuclei (filled circles) and nuclei lighter than Fe-group elements (open diamonds) in the ejecta of SNe Ia.

Table 1
Initial Mass Fractions X of Seed Nuclei for Case A

Nuclide	Abundance
^{32}S	1.92E-04
^{33}S	1.03E-04
^{34}S	7.35E-05
^{36}S	4.99E-05
^{35}Cl	3.79E-05

Note. — (This table is available in its entirety in a machine-readable form in the online journal. A portion is shown here for guidance regarding its form and content.)

Table 2
Initial Mass Fractions X of Seed Nuclei for Case B

Nuclide	Abundance
^{32}S	1.35E-04
^{33}S	8.90E-05
^{34}S	9.04E-05
^{36}S	1.85E-04
^{35}Cl	6.22E-05

Note. — (This table is available in its entirety in a machine-readable form in the online journal. A portion is shown here for guidance regarding its form and content.)

Table 3
Initial Compositions and Average Overproduction Factors of p-nuclei

Case	$X(^{12}\mathrm{C})$	$X(^{16}\mathrm{O})$	$X(^{22}\mathrm{Ne})$	F_0
A1	0.475	0.500	0.023	4657
A2	0.350	0.625	0.023	4606
A3	0.700	0.275	0.023	4777
A4	0.498	0.500	0.000	7621
B	0.475	0.500	0.022	250734

Table 4
Average Overproduction Factors $\langle F \rangle$ Normalized to F_0 for p-nuclei

Nuclide	Case A1	Case A2	Case A3	Case A4	Case B
^{74}Se	1.05E+00	6.87E-01	1.74E+00	2.81E+00	4.94E-02
^{78}Kr	3.67E-01	2.96E-01	5.01E-01	4.98E+00	3.07E-02
^{84}Sr	5.78E-01	5.19E-01	7.68E-01	6.59E+00	6.94E-02
^{92}Mo	1.81E-01	1.74E-01	1.84E-01	5.46E-01	5.40E-02
^{94}Mo	1.32E-01	1.35E-01	1.27E-01	7.66E-02	3.20E-02
^{96}Ru	1.80E-01	1.73E-01	1.83E-01	1.39E-01	6.74E-02
^{98}Ru	5.12E-01	5.21E-01	4.95E-01	3.11E-01	1.55E-01
^{102}Pd	2.09E+00	2.15E+00	2.00E+00	1.26E+00	7.89E-01
^{106}Cd	1.82E+00	1.81E+00	1.79E+00	1.15E+00	8.15E-01
^{108}Cd	1.47E+00	1.51E+00	1.42E+00	8.83E-01	5.20E-01
^{113}In	2.04E-01	2.34E-01	1.71E-01	1.06E-01	7.23E-02
^{112}Sn	1.68E+00	1.76E+00	1.59E+00	9.94E-01	8.51E-01
^{114}Sn	1.64E+00	1.68E+00	1.58E+00	1.02E+00	6.84E-01
^{115}Sn	1.06E-02	1.43E-02	7.36E-03	2.70E-03	3.93E-03
^{120}Te	1.98E+00	1.99E+00	1.92E+00	1.23E+00	9.32E-01
^{124}Xe	2.74E+00	2.88E+00	2.59E+00	1.58E+00	1.76E+00
^{126}Xe	3.41E+00	3.16E+00	3.58E+00	2.51E+00	2.38E+00
^{130}Ba	4.23E+00	4.41E+00	4.01E+00	2.43E+00	3.21E+00
^{132}Ba	3.07E+00	3.17E+00	2.90E+00	1.77E+00	2.43E+00
^{138}La	9.54E-02	1.21E-01	6.30E-02	9.24E-03	8.31E-02
^{136}Ce	7.69E-01	7.75E-01	7.53E-01	4.59E-01	9.18E-01
^{138}Ce	8.03E-01	7.87E-01	7.96E-01	5.03E-01	1.04E+00
^{144}Sm	6.36E-01	6.59E-01	6.06E-01	3.63E-01	1.68E+00
^{152}Gd	1.40E-02	1.55E-02	1.29E-02	8.20E-03	2.25E-02
^{156}Dy	2.81E-01	2.55E-01	3.18E-01	2.58E-01	6.70E-01
^{158}Dy	9.64E-02	9.79E-02	8.55E-02	5.05E-02	1.75E-01
^{162}Er	3.81E-01	3.40E-01	4.21E-01	3.22E-01	1.00E+00
^{164}Er	9.33E-02	9.14E-02	9.05E-02	4.65E-02	2.63E-01
^{168}Yb	1.14E+00	1.07E+00	1.15E+00	7.23E-01	3.38E+00
^{174}Hf	8.10E-01	8.46E-01	7.63E-01	4.69E-01	2.52E+00
^{180}Ta	4.36E-03	7.04E-03	2.32E-03	2.06E-04	7.29E-03
^{180}W	1.49E+00	1.51E+00	1.49E+00	8.67E-01	4.85E+00
^{184}Os	2.61E-01	4.12E-01	9.82E-02	1.19E-02	4.83E-01
^{190}Pt	1.23E-01	1.16E-01	1.23E-01	8.92E-02	4.11E-01
^{196}Hg	6.54E-01	6.39E-01	6.51E-01	4.36E-01	2.57E+00

Note. — All values in respective columns are normalized to different F_0 values, which are listed in Table 3.

Table 5

Overproduction Factors of Ejecta $X_{\mathrm{ejecta}}/X_{\odot}$ for Stable Nuclei from C to Fe and *p*-nuclei

Nuclide	Abundance	Nuclide	Abundance	Nuclide	Abundance
^{12}C	7.66E+00	^{46}Ca	1.79E-03	^{74}Se	3.53E+02
^{13}C	1.51E-08	^{48}Ca	1.15E-06	^{78}Kr	1.23E+02
^{14}N	3.15E-06	^{45}Sc	1.06E+01	^{84}Sr	1.94E+02
^{15}N	3.49E-03	^{46}Ti	1.56E+02	^{92}Mo	6.07E+01
^{16}O	1.06E+01	^{47}Ti	3.45E+00	^{94}Mo	4.44E+01
^{17}O	5.42E-05	^{48}Ti	1.05E+00	^{96}Ru	6.06E+01
^{18}O	1.51E-07	^{49}Ti	7.10E+01	^{98}Ru	1.72E+02
^{19}F	5.20E-05	^{50}Ti	4.86E+00	^{102}Pd	7.03E+02
^{20}Ne	4.93E+00	^{50}V	6.59E+00	^{106}Cd	6.13E+02
^{21}Ne	7.21E-03	^{51}V	5.01E+01	^{108}Cd	4.94E+02
^{22}Ne	8.36E+00	^{50}Cr	3.23E+02	^{113}In	6.85E+01
^{23}Na	3.91E-01	^{52}Cr	3.76E+02	^{112}Sn	5.65E+02
^{24}Mg	3.24E+01	^{53}Cr	1.18E+03	^{114}Sn	5.52E+02
^{25}Mg	8.37E-02	^{54}Cr	5.00E+01	^{115}Sn	3.57E+00
^{26}Mg	2.24E-01	^{55}Mn	4.37E+02	^{120}Te	6.64E+02
^{27}Al	8.26E+00	^{54}Fe	1.53E+03	^{124}Xe	9.21E+02
^{28}Si	1.78E+02	^{56}Fe	3.79E+02	^{126}Xe	1.15E+03
^{29}Si	9.75E+00	^{57}Fe	2.80E+02	^{130}Ba	1.42E+03
^{30}Si	1.39E+02	^{58}Fe	4.12E+01	^{132}Ba	1.03E+03
^{31}P	1.51E+01	^{59}Co	1.02E+02	^{138}La	3.21E+01
^{32}S	1.50E+02	^{58}Ni	8.96E+02	^{136}Ce	2.59E+02
^{33}S	1.76E+02	^{60}Ni	4.08E+02	^{138}Ce	2.70E+02
^{34}S	6.61E+01	^{61}Ni	5.41E+00	^{144}Sm	2.14E+02
^{36}S	1.78E-01	^{62}Ni	7.06E+01	^{152}Gd	4.70E+00
^{35}Cl	3.44E+01	^{64}Ni	2.30E-01	^{156}Dy	9.44E+01
^{37}Cl	2.21E+01	^{63}Cu	5.43E-01	^{158}Dy	3.24E+01
^{36}Ar	2.06E+02	^{65}Cu	3.02E-02	^{162}Er	1.28E+02
^{38}Ar	4.63E+01			^{164}Er	3.14E+01
^{40}Ar	3.59E-02			^{168}Yb	3.84E+02
^{39}K	1.51E+01			^{174}Hf	2.72E+02
^{41}K	1.90E+01			^{180}Ta	1.47E+00
^{40}Ca	4.97E+02			^{180}W	5.01E+02
^{42}Ca	3.81E+01			^{184}Os	8.78E+01
^{43}Ca	1.38E-01			^{190}Pt	4.12E+01
^{44}Ca	4.19E+01			^{196}Hg	2.20E+02

Table 6
Relative Ejected Mass in One SN Event

Type	p-nuclei[a]	^{16}O[a]	^{56}Fe[a]
SN II	45	188	72
SN Ia	638	15	524

Note. — As for values of SNe II, the IMF averages in Tsujimoto et al. 1995 are used.

[a] Values of $M_i/X_{i,\odot}$ for nuclei i and average over p-nuclei.

Table 7
Contributions to the Galactic Contents of p-nuclei

Type	p-nuclei	^{16}O	^{56}Fe
SN II	0.46	2.0	0.75
SN Ia	1	0	0.82

Note. — Ratios of masses that have ever been ejected in the Galaxy by two types of SN events to the corresponding solar mass fractions. Values are normalized so that the p-nuclei for SNe Ia are unity.